High-order harmonic generation in graphene quantum dots in the field of an elliptically polarized pulse

Suresh Gnawali [*] and Vadym Apalkov [†]
Department of Physics and Astronomy, Georgia State University, Atlanta, Georgia 30303, USA

(Received 16 December 2023; revised 16 March 2024; accepted 27 March 2024; published 10 April 2024)

We study theoretically the generation of high-order harmonics in graphene quantum dots placed in the field of an elliptically polarized ultrashort pulse. The generated high-order harmonics are sensitive to the pulse's ellipticity and its amplitude. The intensities of high-order harmonics become very sensitive to the ellipticity of an incident pulse when its polarization gets close to a circular one, and some high-order harmonics become strongly suppressed for a circularly polarized incident pulse. The suppressed harmonic orders depend on the symmetry of the quantum dot systems. For triangular quantum dots, which have D_{3h} symmetry, every third harmonic is suppressed, while for hexagonal quantum dots with D_{6h} symmetry, such suppression is observed for every sixth harmonic, and the even-order harmonics are suppressed for all ellipticities of the incident pulse due to an additional inversion symmetry of the hexagonal quantum dots. The ellipticities of the generated high-order harmonics also show strong nonmonotonic dependence on the ellipticity of an incident pulse, in which the dependence becomes stronger for high pulse amplitudes.

DOI: 10.1103/PhysRevB.109.165121

I. INTRODUCTION

There has been growing interest in theoretical and experimental studies of optical nonlinearities of solids, including high-order harmonic generation (HHG) and nonlinear absorption and scattering, among other things [1–12]. Recently, HHG in two-dimensional (2D) materials, including graphene [13–16] and transition metal dichalcogenides [17], has drawn much attention due to their promising optical and electronic properties compared to three-dimensional solids. Several nanostructures, including graphene quantum dots (GQDs) [18] and graphene nanoribbons [19], were studied extensively to overcome the limitation due to the lack of a band gap in semimetallic graphene. Band gap tunability in GQDs can be achieved by varying the lateral shape, size, and type of edge, making GQDs more suitable for nonlinear optical systems [20]. The generation of high-order harmonics and its dependence on relaxation processes have been reported numerically in hexagonal GQDs with just 24 atoms [21]. Recent studies have also reported that HHG in GQDs with triangular [22,23] and rectangular [24] geometries shows several exciting properties. Namely, in Ref. [23], strong suppression of even-order harmonics has been reported in triangular GQDs, which have an even number of edge states. The suppression of even harmonics is realized when half of the edge states are initially, i.e., before the pulse, occupied.

While the HHG is mainly studied for linearly polarized optical pulses, general polarization of the incident optical pulse, e.g., elliptical polarization, provides unique opportunities to explore, investigate, and control strong light-matter interactions in solids and tune their nonlinear optical response. The polarization degree of freedom enables excellent insight into the study of the fundamental aspects of light-matter interaction and time-varying polarization states, which further opens the door to control attoscience coherent techniques, including spectroscopy, and would be a great candidate to control tabletop harmonic processes, including ultraviolet and x-ray spectral regions [25–27]. Recently, the dependence of HHG on the ellipticity of an incident pulse was used to probe the molecular chirality on a subfemtosecond timescale [28]. Furthermore, elliptical polarization enables gating schemes, including polarization gating and double optical gating, to generate attosecond XUV pulses, which study the electron dynamics in atoms, molecules, and solids [29–31].

The elliptical polarization of the laser driver field has opened up several interesting physical phenomena in gases. In contrast, interactions of such pulses with nanosystems of solids are largely unexplored, hindering the possibility of exploitation of experimental techniques for solid-state devices [27]. Therefore, studying the ellipticity dependence of light-matter interactions in 2D materials and their quantum dots (QDs) would lead to new insight into the nonlinear optical properties of these systems.

In 2011, Ghimire *et al.* reported through an experimental study of the bulk ZnO system that emitted high-order harmonics are less sensitive to ellipticity [32] of the optical pulse compared to gases [33,34]. However, under circular polarization of the incident pulse, the generation of high-order harmonics is strongly suppressed despite strong field ionization [32]. Later, Liu *et al.*, conducting a theoretical study of the same material, showed a monotonic decrease in harmonic yield with increasing ellipticity of the driving pulse [35].

On the contrary, experimental work on the MgO system revealed a strong dependence of HHG yield on the ellipticity

[*] sgnawali1@student.gsu.edu
[†] vapalkov@gsu.edu

of the incident pulse, including a significant signal for circular polarization [36]. The authors showed that the maximum harmonic yield, in some cases, can be reached not for linear polarization but for polarization with a finite value of the ellipticity. Later, the enhancement of HHG in graphene by an elliptically polarized driving pulse was also reported [37,38]. Furthermore, circularly polarized extreme ultraviolet HHG in graphene was reported using first-principles simulation within time-dependent density functional theory [39]. These results revealed that circularly polarized driver pulses do not permanently prohibit harmonic generation from specific crystals and 2D materials. There are some proposals for solids to explain maximum harmonic yield at finite ellipticity of the incident pulse in a semimetal regime of the crystal [40].

Quantum dots are systems that have properties of both solids and atoms; i.e., they have discrete energy spectra which are determined by the symmetry of the dots, and also, they have quasispatial periodicity of solids. Interaction of such quantum dots with an incident optical pulse should be sensitive to the polarization of the pulse, i.e., its ellipticity. Here, we consider a special type of quantum dots: graphene quantum dots. Such quantum dots can have different symmetries; e.g., triangular GQDs have D_{3h} symmetry, while hexagonal GQDs have D_{6h} symmetry. The symmetry of the GQD determines its nonlinear optical response, e.g., by suppressing the generation of some harmonics. Below we theoretically study the nonlinear ultrafast dynamics of GQDs within the density matrix approach, which allows us to include the relaxation processes within the GQDs phenomenologically.

The paper is organized as follows. In Sec. II, we introduce the model and main equations. In Sec. III, the results are discussed, which are further summarized in the concluding Sec. IV.

II. MATH AND EQUATIONS

The system of a GQD placed in the field of a short optical pulse is described by a time-dependent Hamiltonian with the following form:

$$H(t) = H_0 + H'(t), \tag{1}$$

where H_0 is the field-free Hamiltonian that describes the GQD system within the scope of the tight-binding model,

$$H_0 = -t \sum_{\langle ij \rangle} (\hat{c}_i^\dagger \hat{c}_j + \text{H.c.}), \tag{2}$$

where i and j label the sites of the QD, $\hat{c}_i^\dagger$ and $\hat{c}_i$ are creation and annihilation operators for an electron at site i, and $t = -2.8$ eV is the hopping integral. We also assume that the on-site energies are zero. Numerical diagonalization of the tight-binding Hamiltonian for a GQD consisting of N atoms gives N levels with wave functions ψ_n and corresponding energies E_n. The wave functions and the energy spectra are obtained numerically.

The Hamiltonian $H'(t)$ describes the interaction of the electron system with the optical field as follows:

$$H'(t) = -e \sum_i \hat{c}_i^\dagger \hat{c}_i \mathbf{r}_i \cdot \mathbf{F}(t), \tag{3}$$

where $\mathbf{r}_i$ is the position of the ith atom and $\mathbf{F}(t)$ is the time-dependent electric field of the optical pulse. Below we consider an elliptically polarized pulse, for which the time-dependent electric field is defined as

$$\mathbf{F}(t) = F_x(t)\hat{\mathbf{e}}_x + F_y(t)\hat{\mathbf{e}}_y, \tag{4}$$

where

$$\begin{aligned} F_x(t) &= F_{0,x} e^{-(t/\tau_0)^2} \cos(\omega_0 t), \\ F_y(t) &= F_{0,y} e^{-(t/\tau_0)^2} \sin(\omega_0 t), \end{aligned} \tag{5}$$

and

$$F_{0,x} = \frac{F_0}{\sqrt{1+\epsilon^2}}, \quad F_{0,y} = \frac{\epsilon F_0}{\sqrt{1+\epsilon^2}}. \tag{6}$$

Here, F_0, ϵ, ω_0, and τ_0, are the amplitude, ellipticity, frequency, and duration of an elliptically polarized optical pulse. The pulse is linearly (circularly) polarized for $\epsilon = 0$ ($\epsilon = 1$). Thus, the driver ellipticity ϵ corresponding to the incident laser pulse is defined as

$$\epsilon = \frac{F_{0,y}}{F_{0,x}}. \tag{7}$$

We study the electron dynamics of the electron system of GQDs using the time evolution of the density operator $\hat{\rho}$, which is determined by the following density matrix equation:

$$\frac{d\hat{\rho}}{dt} = \frac{i}{\hbar}[\hat{\rho}, H] = \frac{i}{\hbar}[\hat{\rho}, H_0] + \frac{i}{\hbar}[\hat{\rho}, H'], \tag{8}$$

where $[\hat{A}, \hat{B}]$ is the commutator of operators $\hat{A}$ and $\hat{B}$.

Taking the matrix elements of the left- and right-hand sides of Eq. (8) between the states ψ_n of the field-free Hamiltonian H_0, we obtain the following system of equations for the density matrix:

$$\dot{\rho}_{mn} = i\omega_{mn}\rho_{mn} + \frac{i}{\hbar}\sum_k (\rho_{mk}H'_{kn} - H'_{mk}\rho_{kn}), \tag{9}$$

where $\omega_{mn} = \frac{(E_n - E_m)}{\hbar}$, E_n is the energy corresponding to state ψ_n, $\rho_{mn} = \langle \psi_m | \hat{\rho} | \psi_n \rangle$, $H'_{kn} = -\mathbf{D}_{kn}\mathbf{F}(t)$, and $\mathbf{D}_{kn} = e\langle \psi_k | \hat{\mathbf{r}} | \psi_n \rangle$ is the dipole matrix element of the dipole operator $e\hat{\mathbf{r}}$.

Employing the density matrix approach provides an opportunity to incorporate the relaxation process into our model through the corresponding phenomenological relaxation rates. To address the relaxation process corresponding to dipole decay we introduce the dephasing time τ, which we assume is the same for all nondiagonal matrix elements of the density matrix. Below we set the dephasing time at $\tau = 10$ fs. Experimentally, the relaxation time that was reported for a graphene monolayer is around 10–20 fs [41–47]. Although our system is a finite-size graphene QD, we assume below that the same relaxation, i.e., dephasing, time is around 10 fs.

With the relaxation processes, the density matrix equation (9) takes the following form:

$$\begin{aligned} \dot{\rho}_{mn} = i\omega_{mn}\rho_{mn} + \frac{i}{\hbar}\sum_k (\rho_{mk}H'_{kn} - H'_{mk}\rho_{kn}) \\ - (1 - \delta_{nm})\rho_{mn}/\tau, \end{aligned} \tag{10}$$

where δ_{nm} is the Kronecker delta symbol.

With the density matrix expressed in the interaction representation,

$$\tilde{\rho}_{mn} = \rho_{mn} e^{-i\omega_{mn}t}, \tag{11}$$

the system of equations (10) takes the following form:

$$\dot{\tilde{\rho}}_{mn} = \frac{i}{\hbar}\sum_k \left[\tilde{\rho}_{mk} e^{i\omega_{nk}t} H'_{kn} - H'_{mk}\tilde{\rho}_{kn} e^{i\omega_{km}t}\right] - (1-\delta_{nm})\tilde{\rho}_{mn}/\tau. \tag{12}$$

We solve the system of differential equations (12) numerically using the ODEINT library, which is a collection of different numerical algorithms to solve initial value problems of ordinary differential equations [48]. The initial conditions are that, before the pulse, all valence band (VB) states are occupied and all conduction band (CB) states are empty, i.e., $\tilde{\rho}_{nn} = 1$ if $n \in$ VB and $\tilde{\rho}_{nn} = 0$ if $n \in$ CB.

With the known solution of the density matrix equation (12), the time-dependent dipole moment can be calculated from the following expression:

$$\mathbf{d}(t) = \sum_{mn} \tilde{\rho}_{mn}(t) e^{i\omega_{mn}t} \mathbf{D}_{nm}. \tag{13}$$

The time variation of the dipole moment determines the radiation of the system. At a given frequency ω, the intensity of the corresponding radiation is obtained from the following expression:

$$I(\omega) = I_x(\omega) + I_y(\omega), \tag{14}$$

where

$$I_x(\omega) = \frac{\mu_0\omega^2}{12\pi c}[|\mathcal{F}_\omega[\dot{d}_x]|^2, \quad I_y(\omega) = \frac{\mu_0\omega^2}{12\pi c}|\mathcal{F}_\omega[\dot{d}_y]|^2]. \tag{15}$$

Here, $\mathcal{F}_\omega[\dot{d}_x]|^2$ and $\mathcal{F}_\omega[\dot{d}_y]|^2]$ are frequency Fourier transforms of the time derivatives of the corresponding components of the dipole moment.

The order of the generated high-order harmonic is defined in units of ω_0, i.e.,

$$N_\omega = \frac{\omega}{\omega_0}. \tag{16}$$

The generated high-order harmonics in the field of an elliptically polarized pulse are also elliptically polarized. From our numerical analysis, we found that the difference between the phases of the Fourier transforms of the derivative of the y and x components of the dipole moment, i.e., $\mathcal{F}_\omega[\dot{d}_y]$ and $\mathcal{F}_\omega[\dot{d}_x]$, is close to 90°, which shows that the x and y axes are the axes of the corresponding polarization ellipse of high-order harmonics. In this case, we define the corresponding ellipticity $\epsilon(N_\omega)$ of the N_ωth harmonics using the following expression:

$$\epsilon(N_\omega) = \frac{\widetilde{F}_y(N_\omega)}{\widetilde{F}_x(N_\omega)} = \sqrt{\frac{I_y(\omega)}{I_x(\omega)}}, \tag{17}$$

where $\widetilde{F}_x(N_\omega)$ and $\widetilde{F}_y(N_\omega)$ are the x and y components of the electric field of the generated N_ωth harmonics. Such a defined ellipticity can be greater than 1 and also determines the orientation of the polarization ellipse; i.e., if $\epsilon(N_\omega) < 1$ [$\epsilon(N_\omega) > 1$], then the principal axis of the polarization ellipse is the x axis (y axis).

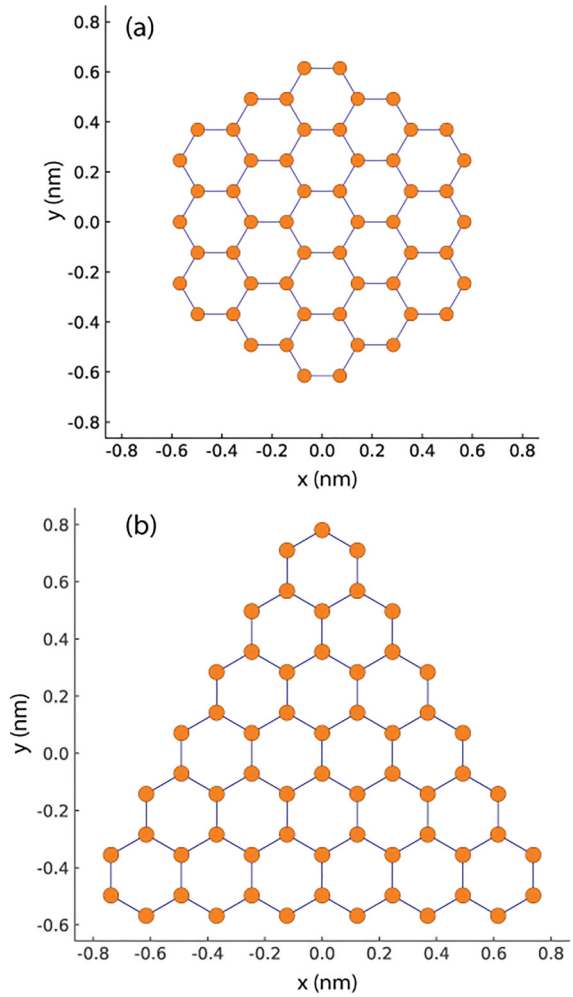

FIG. 1. Hexagonal and triangular graphene quantum dots. (a) The hexagonal dots consist of 54 atoms, and (b) triangular dots possess 61 atoms. The distance between the nearest-neighbor atoms is $a = 1.42$ Å.

III. RESULTS AND DISCUSSION

Below, we study two types of GQDs, hexagonal and triangular, which have different point symmetries. The corresponding GQDs are shown in Fig. 1. The hexagonal QD consists of 54 carbon atoms and has D_{6h} symmetry, while the triangular QD has 61 atoms and the corresponding symmetry is D_{3h}. The triangular QD also has zigzag edges. We consider only two sizes of QDs to identify the symmetry-related effects in the nonlinear optical response of the systems.

The energy spectra of the triangular and hexagonal QDs are shown in Fig. 2. Due to dimensional quantization, both systems have finite band gaps, which are 1.91 eV for the hexagonal QD and 1.87 eV for the triangular QD. The triangular QD with zigzag edges also has degenerate in-gap edge states with zero energy, which are marked in Fig. 2. The bulk states of both triangular and hexagonal GQDs belong to either one- or two-dimensional irreducible representations of the corresponding symmetry groups, D_{3h} and D_{6h}.

In all calculations below, we keep the same frequency of the pulse, 1 eV, which is less than the band gap for both GQD

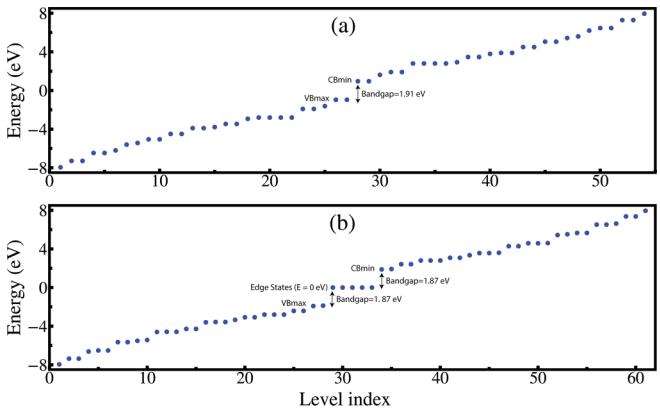

FIG. 2. Energy spectra of (a) a hexagonal GQD and (b) a triangular GQD. For a triangular QD, zero-energy states are the edge states, as shown. The valence and conduction band edge states and the corresponding band gaps are marked for each GQD. Levels with negative and positive energies correspond to the valence band and conduction band states, respectively.

systems. We change the amplitude F_0 of the pulse, with a maximum amplitude of up to 0.3 V/Å. The radiation spectra of triangular and hexagonal GQDs are shown in Fig. 3 for different ellipticity values of the incident pulse. The radiation spectra clearly follow the symmetries of the systems. No even-order harmonics are realized for the hexagonal QD, which has inversion symmetry, while for the triangular QD, both even-order and odd-order harmonics are clearly visible in the radiation spectrum. Another symmetry-related feature is the suppression of some high-order harmonics when the incident pulse becomes circularly polarized. Namely, the triangular GQD has D_{3h} symmetry with a rotational element of C_3, and the orders of high-order harmonics that are suppressed are 3, 6, 9, ..., i.e., $3 + 3m$, where m is an integer. The hexagonal GQD has D_{6h} symmetry, which results in the suppression of high-order harmonics with orders 3, 9, 15, ..., i.e., $3 + 6m$, where m is an integer. The suppression of the high-order harmonics, mentioned above, is realized when the ellipticity gets close to 1, which corresponds to a circularly polarized pulse. For all field amplitudes, the suppression of the corresponding harmonics is clearly pronounced. Also, for the hexagonal QD, the harmonic orders of 6, 12, 18, and so on, i.e., even-order harmonics from the set of $3 + 3m$, are suppressed for all ellipticities due to the inversion symmetry of such a quantum dot. For the high-order harmonics, which do not show any suppression for a circularly polarized pulse, the dependence of an incident pulse on the ellipticity is weak. The cutoff frequency, which is analyzed in detail below, also has a weak dependence on the ellipticity of the pulse.

To illustrate the suppression of the corresponding high-order harmonics for a circularly polarized pulse, we show in Fig. 4 the intensities of the first few harmonics as a function of the ellipticity of an incident pulse. The data show that the suppression of the corresponding harmonics occurs mainly in the range from $\epsilon > 0.9$. The suppression is less pronounced for the triangular QD [see Fig. 4(b)], which has a larger number of atoms than the hexagonal QD. Namely, for the hexagonal QD [see Fig. 4(a)], for all harmonics, the corresponding intensities are suppressed by 4–5 orders of magnitude, while for the triangular QD, only the third-order harmonics is suppressed by 4 orders of magnitude and all other higher-order harmonics are suppressed by 2–3 orders of magnitude.

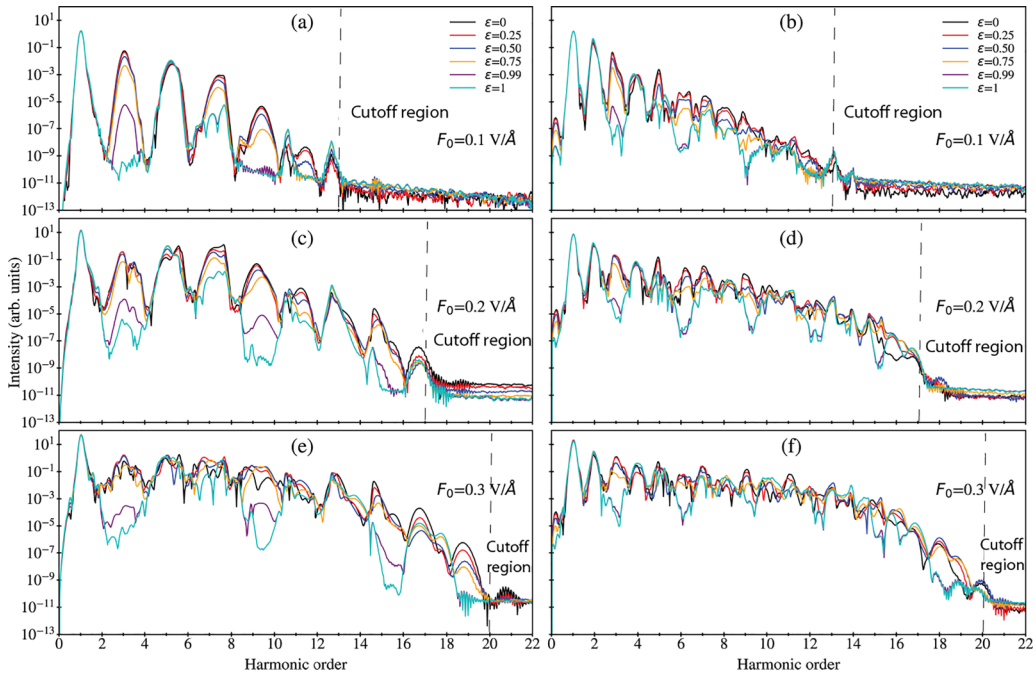

FIG. 3. Emission spectra of graphene QDs: (a), (c), and (e) hexagonal QD and (b), (d), and (f) triangular QDs. In each panel, different lines correspond to different ellipticities of the incident pulse. The pulse frequency is $\hbar\omega_0 = 1$ eV. The field amplitude of the incident pulse is (a) and (b) $F_0 = 0.1$ V/Å, (c) and (d) 0.2 V/Å, and (e) and (f) 0.3 V/Å. The dephasing time is $\tau = 10$ fs. The intensity is shown on a logarithmic scale.

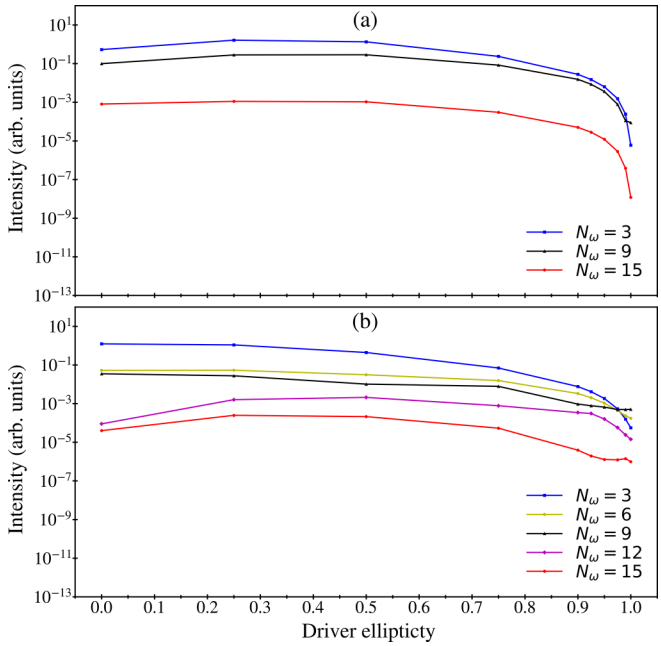

FIG. 4. Intensities of high-order harmonics as a function of the ellipticity of the incident pulse. The results are shown for (a) a hexagonal QD and (b) a triangular QD. The pulse frequency is $\hbar\omega_0 = 1$ eV, and its amplitude is 0.3 V/Å. The dephasing time is $\tau = 10$ fs. The results are shown for harmonic orders of 3, 9, and 15 in (a) and 3, 6, 9, 12, and 15 in (b) as marked. The intensity is shown on a logarithmic scale.

The emitted high-order harmonics are also elliptically polarized, and their polarization is characterized by the corresponding ellipticity. The dependence of the ellipticities of different high-order harmonics on the ellipticity of the incident pulse is shown in Fig. 5 for the first four odd harmonics ($N_\omega = 1$, 3, 5, and 7). For a linearly polarized optical pulse, i.e., $\epsilon = 0$, the situation is different for the hexagonal and triangular QDs. For the hexagonal QD [see Figs. 5(a) and 5(c)], for which the x axis is the axis of symmetry, the optical pulse that is linearly polarized along the x direction generates only the x component of the dipole moment, resulting in high-order harmonics which are linearly polarized with zero ellipticity. For the triangular QD, the x axis is not the axis of symmetry. In this case, a linearly polarized pulse generates both the x and y components of the dipole moment, resulting in the emission of high-order harmonics which are elliptically polarized with small, but finite, ellipticity [see Figs. 5(b) and 5(d)].

Also, the ellipticity of the first-order harmonics, the frequency of which is the same as the frequency of the incident pulse, is almost the same as the ellipticity of the incident pulse. The difference between them is more pronounced for the high field amplitude of 0.3 eV/Å [see Figs. 5(c) and 5(d)]; this difference is related to the nonlinear dynamics of the electron system in the field of the pulse, where the nonlinearity becomes more pronounced for higher field amplitudes.

For the high-order harmonics, the unique property of their ellipticities is that they are larger than the ellipticity of the incident pulse. For some cases, the ellipticities of high-order harmonics even exceed 1, which means that, while for an incident pulse the x component of the optical field is greater than the y component, for the high-order harmonics, the x component of the generated field becomes less than the corresponding y component. The enhancement of the ellipticity of high-order harmonics is not related to the system's symmetry; i.e., the behavior is similar for both hexagonal and triangular quantum dots. At the same time, for the hexagonal quantum dot [see Figs. 5(a) and 5(c)], the enhancement of the ellipticities of high-order harmonics is more pronounced than for the triangular quantum dot. Also, the tendency with increasing the amplitude of the incident pulse is that the largest ellipticity is observed at smaller-order harmonics when the amplitude of the pulse increases. For example, for a field amplitude of 0.1 V/Å, the maximum ellipticity is realized for the fifth and seventh harmonics, while for a field amplitude of 0.3 V/Å, the maximum ellipticity is realized for the third harmonic.

While the hexagonal quantum dot has inversion symmetry, which results in the suppression of even-order harmonics, the triangular quantum dot does not have such symmetry, and odd-order harmonics are generated in the field of an elliptically polarized pulse. The ellipticities of the corresponding harmonics are shown in Fig. 6. For a linearly polarized pulse along the x direction, i.e., for $\epsilon = 0$, the emitted even-order harmonics are linearly polarized along the y axis, which follows from the reflection symmetry of the triangular quantum dot with respect to the y axis. For our definition of the ellipticity, this polarization results in the infinite ellipticity of the even-order harmonics for $\epsilon = 0$. For the finite ellipticity of the incident pulse, $\epsilon > 0$, the ellipticities of the even-order harmonics are mainly greater than the ellipticity of the incident pulse. Also, for a circularly polarized incident pulse, $\epsilon = 1$, the emitted harmonics are circularly polarized.

For a triangular graphene QD with zigzag edges, there are degenerate edge states with zero energy. Above, we considered the situation in which only the valence band states are initially populated. For such a quantum dot, there is another possibility when both the valence and edge states are populated before the pulse. A comparison of the emission spectra for these two cases is presented in Fig. 7. The results are identical, which is a manifestation of the particle-hole symmetry for these two systems. Namely, the situation in which only the valence band states are initially populated by electrons is identical to the situation in which only the conduction band states are initially populated by holes, i.e., the valence band and edge states are populated by electrons before the pulse. This symmetry is presented in the tight-binding model of graphene QDs considered above.

One of the important characteristics of the emission spectra is the cutoff frequency, i.e., the maximum frequency that can be generated by the system placed in the field of a pulse. The cutoff frequency as a function of the ellipticity ϵ of the incident pulse is shown in Fig. 8. The cutoff frequency has weak dependence on ϵ, with some large changes observable near $\epsilon \approx 0.5$. Namely, for the hexagonal QD and the large field amplitude, $F_0 = 0.3$ V/Å, the cutoff frequency decreases when the driver ellipticity increases from $\epsilon = 0.25$ to 0.5 and is constant at larger values of ϵ, $\epsilon > 0.5$. At a smaller field amplitude, $F_0 = 0.1$ V/Å, the cutoff frequency shows nonmonotonic dependence within the interval of $0.25 < \epsilon < 0.75$, with the maximum at $\epsilon = 0.5$. For the triangular QD,

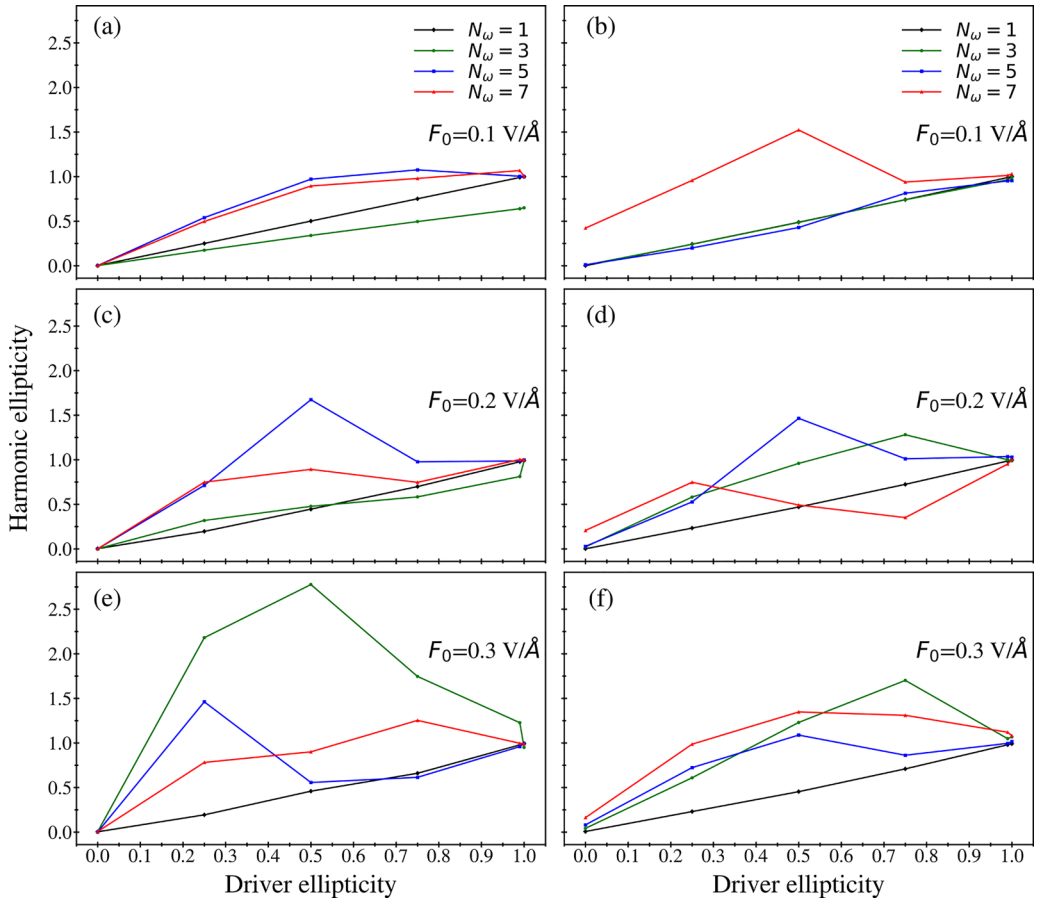

FIG. 5. Ellipticities of the first four odd high-order harmonics ($N_\omega = 1$, 3, 5, and 7) as a function of the ellipticity of the incident pulse. The results are shown for (a) and (c) a hexagonal QD and (b) and (d) a triangular QD. The field amplitude is (a) and (b) 0.1 V/Å, and (c) and (d) 0.3 V/Å. The pulse frequency is $\hbar\omega_0 = 1$ eV. The dephasing time is $\tau = 10$ fs.

the cutoff frequency decreases for $\epsilon > 0.75$, with the smallest value being realized for a driver ellipticity close to 1.

With increasing field amplitude, the cutoff frequency increases; i.e., more harmonics are generated, which is expected behavior for systems interacting with an optical pulse. Also, for both types of QDs, triangular and hexagonal, the cutoff frequency is almost the same, which suggests that the cutoff frequency has real sensitivity to the geometry of QDs.

The generation of high-order harmonics is a manifestation of nonlinear electron dynamics in graphene QDs placed in the field of an optical pulse. Such electron dynamics can also be characterized by the population of excited QD states, i.e., conduction band and edge states, during the pulse and after the pulse. In Fig. 9 the total population of excited QD states is shown as a function of time. While it is an integral characteristic of the electron dynamics, the results are different for a linearly polarized incident pulse and a circularly polarized pulse. For a linearly polarized pulse, shown by blue lines in Fig. 9, the population of the excited QD states shows an oscillatory behavior during the pulse, while such behavior is strongly suppressed for a circularly polarized pulse, which is illustrated by the red lines. This behavior is consistent with suppression of the high-order harmonics reported above for a circularly polarized incident pulse. For all cases, the electron dynamics is highly irreversible; i.e., the residual population of the excited states is comparable to the corresponding maximum population during the pulse. Also, in terms of the total population of the excited states, there is no fundamental difference between the triangular and hexagonal quantum dots. For both cases, the results show similar behavior because both systems have comparable band gaps around 1.9 eV.

Another characteristic of the electron dynamics is a residual population of the excited states of a QD after the pulse. Such a population is shown in Fig. 10 for both triangular and hexagonal QDs and for two polarizations of the incident pulse: linear and circular ones. While for the total population of the excited states shown in Fig. 9 there is no difference between the two types of QDs, for the populations of individual levels shown in Fig. 10, there is a fundamental difference. Namely, for the triangular QD [see Figs. 10(b) and 10(d)], there is a large population of edge states and a relatively small population of conduction band states, while for the hexagonal QD, the population of conduction band states is relatively large. This behavior is related to the different natures of the band gaps in these two QD systems. For the hexagonal QD, the band gap of 1.91 eV is between the valence band states and the conduction band states, while for the triangular QD, the band gap of 1.89 eV is between the valence band states and the edge states of the system. In terms of the dependence of an incident pulse on polarization, for both types of QDs,

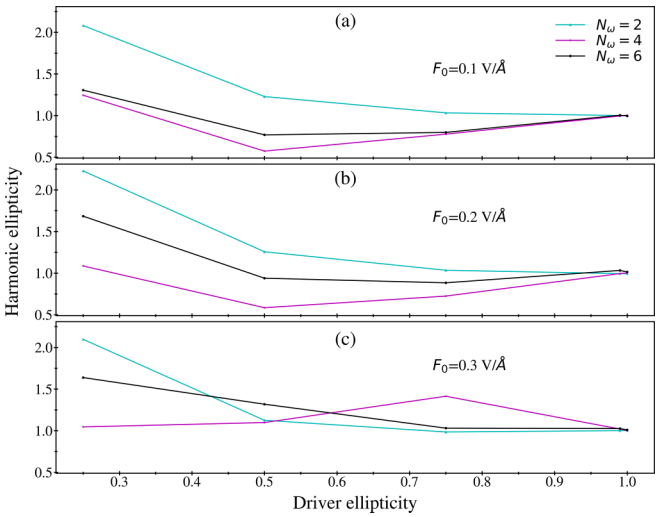

FIG. 6. Ellipticities of the first three even-order harmonics ($N_\omega =$ 2, 4, and 6) as a function of the ellipticity of the incident pulse. The results are shown for a triangular QD and field amplitudes of (a) 0.1, (b) 0.2, and (c) 0.3 V/Å. The data are shown only for an ellipticity ϵ of the incident pulse greater than 0.2, while for small values of ϵ, the ellipticities of the even harmonics are very large, illustrating the fact that for a linearly polarized pulse in the x direction, the even harmonics are linearly polarized in the y direction. The pulse frequency is $\hbar\omega_0 = 1$ eV. The dephasing time is $\tau = 10$ fs.

the lower-energy excited states become more populated for a circularly polarized pulse. Namely, for the triangular QD, the edge states become more populated after a circularly polarized pulse, while for the hexagonal QD, the excited states near the edge of the conduction band are more populated for a circularly polarized pulse compared to a linearly polarized pulse.

IV. CONCLUSION

The emission spectra of graphene quantum dots in the field of an optical pulse depend not only on its intensity but also on its polarization. Namely, for an elliptically polarized pulse, the ellipticity of the pulse can be used as a tuning parameter to change the generation of high-order harmonics in QD systems. In the present paper, we considered two types of graphene QDs: hexagonal and triangular QDs, which have D_{6h} and D_{3h} symmetries, respectively. The radiation spectra of such QDs show strong sensitivity to the ellipticity of an optical pulse when its polarization becomes close to circular. Such sensitivity is visible as the suppression of some high-order harmonics in the radiation spectra. The orders that are suppressed are determined by the symmetry of the QD; for a triangular QD, every third harmonic is suppressed, while for a hexagonal QD, every sixth harmonic is suppressed. While for small field amplitudes the suppression of the corresponding harmonics is realized mainly for a circularly polarized pulse, for large field amplitude, the suppression occurs also for an elliptically polarized pulse with ellipticities that are in some range close to a circularly polarized pulse. Also, for a hexagonal QD, which has inversion symmetry, all even-order harmonics are suppressed for all ellipticities of an optical pulse and not only for a circularly polarized pulse.

Interaction of an elliptically polarized pulse with graphene QDs also generates elliptically polarized radiation. The ellipticities of the corresponding high-order harmonics depend on the parameters of the incident pulse, and in some cases, for large enough harmonic orders or large intensities of an

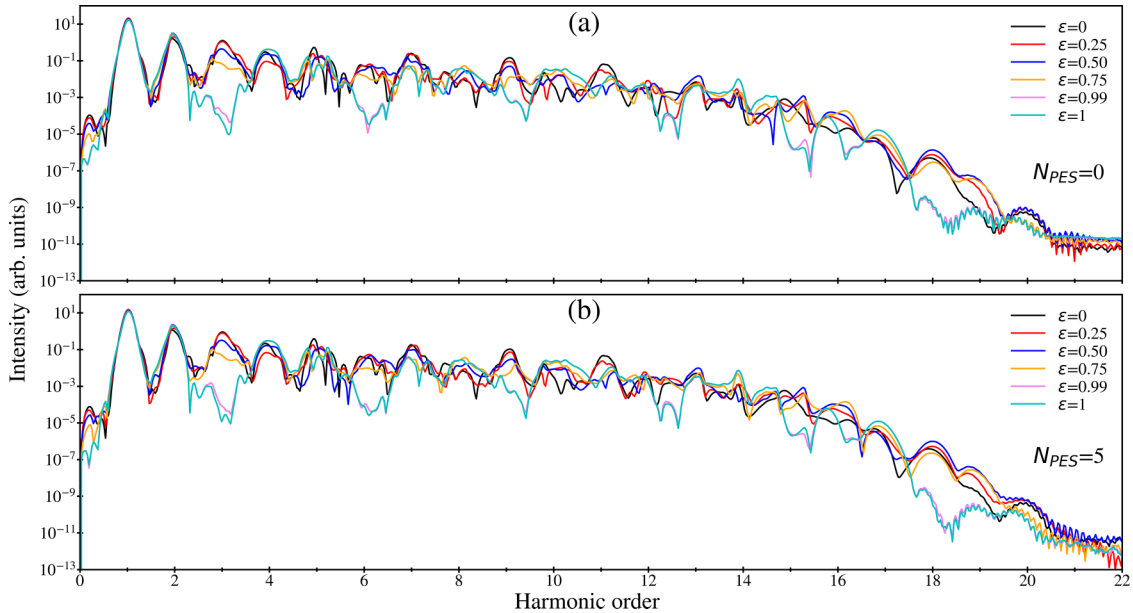

FIG. 7. Emission spectra of a triangular graphene QD. In each panel, different lines correspond to different ellipticities of the incident pulse. In (a), only the valence band states with negative energies are occupied before the pulse, while in (b), both the valence band states and all edge states are initially populated. The parameter $N_{\rm PES}$ shows the number of populated edge states. The pulse frequency is $\hbar\omega_0 = 1$ eV. The field amplitude of the incident pulse is $F_0 = 0.3$ V/Å. The dephasing time is $\tau = 10$ fs. The intensity is shown on a logarithmic scale.

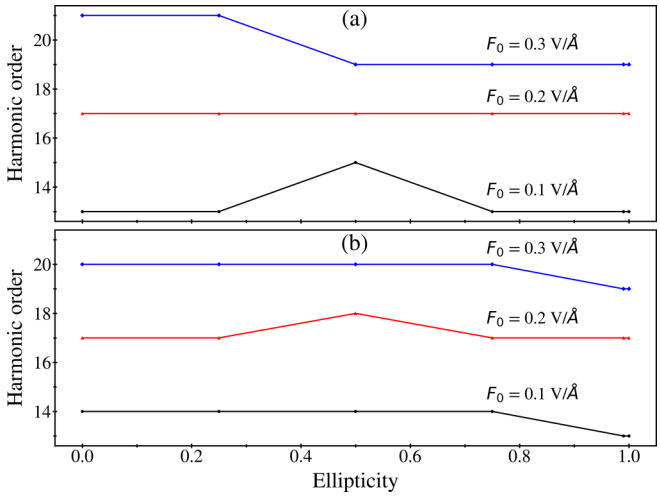

FIG. 8. Cutoff frequency as a function of the ellipticity of the incident pulse. The results are shown for (a) a hexagonal QD and (b) a triangular QD. The frequency of the pulse is $\hbar\omega_0 = 1$ eV. The field amplitudes are shown next to the corresponding lines.

incident pulse, the corresponding polarization ellipse of high-order harmonics is effectively rotated by 90° compared to the polarization ellipse of the incident pulse.

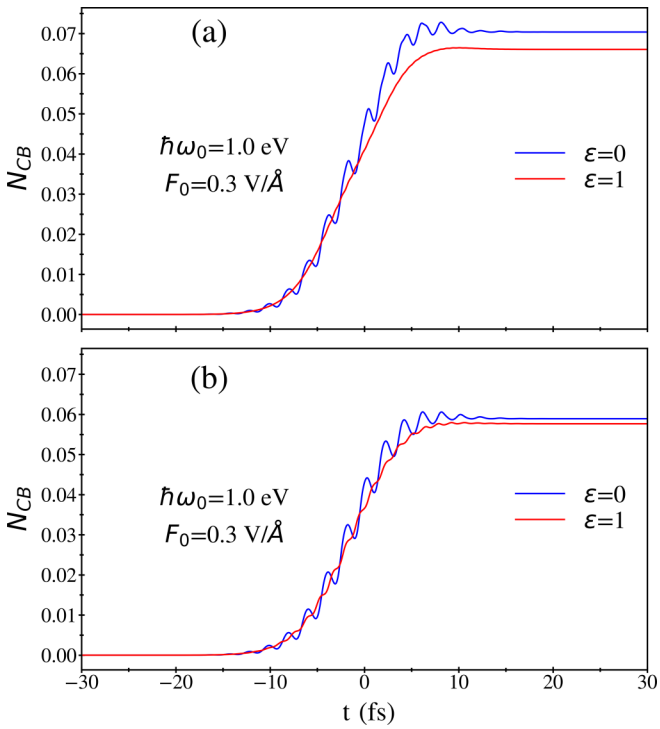

FIG. 9. Conduction band populations of graphene QDs as a function of time. The results are shown for (a) the hexagonal QD and (b) the triangular QD. In each panel, the results are shown for a linearly polarized pulse, $\epsilon = 0$, and a circularly polarized pulse, $\epsilon = 1$, by the blue and red lines, respectively. The frequency of the pulse is $\hbar\omega_0 = 1$ eV, and the field amplitude is 0.3 V/Å.

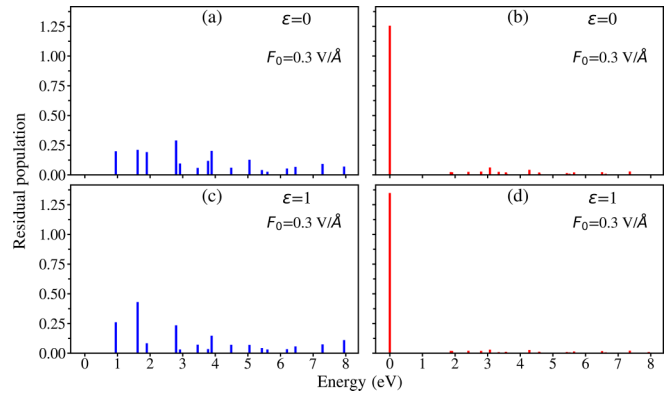

FIG. 10. Residual populations of individual excited states of graphene QDs. The results are shown (a) and (c) for the hexagonal QD and (b) and (d) for the triangular QD. The polarization of an incident pulse is linear in (a) and (b) and circular in (c) and (d). For the triangular QD, the results at zero energy correspond to populations of initially unoccupied edge states of the QD. The frequency of the pulse is $\hbar\omega_0 = 1$ eV, and the field amplitude is 0.3 V/Å.

We studied the ultrafast electron dynamics of graphene QDs under an elliptically polarized pulse. The harmonic intensities depend on the amplitude of the optical pulse, its ellipticity, and the symmetry of the QD. The symmetry of the QD system plays a vital role in the occurrence of even- or odd-order harmonics. Here, we observed only odd harmonics for the hexagonal dots, which possess D_{6h} symmetry, while for triangular dots with D_{3h} symmetry, both the even- and odd-order harmonics were observed. More importantly, the suppression of the harmonics was observed for both hexagonal and triangular dots. Such suppression of the high-order harmonics by varying the ellipticity of the incident pulse could provide an excellent way to control the HHG in graphene QDs and other 2D systems. The harmonic conversion efficiency for graphene QDs is of the order of 10^{-14} per quantum dot. To enhance the conversion efficiency, an array of the corresponding quantum dots should be considered.

Thus, for graphene quantum dots interacting with an elliptically polarized optical pulse, both the intensity and the polarization of the generated high-order harmonics can be controlled by tuning the ellipticity of an incident pulse.

ACKNOWLEDGMENTS

Major funding was provided by Grant No. DE-FG02-01ER15213 from the Chemical Sciences, Biosciences and Geosciences Division, Office of Basic Energy Sciences, Office of Science, U.S. Department of Energy. Numerical simulations were performed using support from Grant No. DE-SC0007043 from the Materials Sciences and Engineering Division of the Office of the Basic Energy Sciences, Office of Science, U.S. Department of Energy.

[1] M. Lewenstein, P. Balcou, M. Y. Ivanov, A. L'Huillier, and P. B. Corkum, Theory of high-harmonic generation by low-frequency laser fields, Phys. Rev. A **49**, 2117 (1994).

[2] G. Vampa, C. R. McDonald, G. Orlando, D. D. Klug, P. B. Corkum, and T. Brabec, Theoretical analysis of high-harmonic generation in solids, Phys. Rev. Lett. **113**, 073901 (2014).

[3] E. Goulielmakis and T. Brabec, High harmonic generation in condensed matter, Nat. Photon. **16**, 411 (2022).

[4] B. Dromey *et al.*, High harmonic generation in the relativistic limit, Nat. Phys. **2**, 456 (2006).

[5] S. Kim, J. Jin, Y.-J. Kim, I.-Y. Park, Y. Kim, and S.-W. Kim, High-harmonic generation by resonant plasmon field enhancement, Nature (London) **453**, 757 (2008).

[6] G. Vampa *et al.*, Plasmon-enhanced high-harmonic generation from silicon, Nat. Phys. **13**, 659 (2017).

[7] L. Yue and M. B. Gaarde, Characterizing anomalous high-harmonic generation in solids, Phys. Rev. Lett. **130**, 166903 (2023).

[8] E. N. Osika, A. Chacón, L. Ortmann, N. Suárez, J. A. Pérez-Hernández, B. Szafran, M. F. Ciappina, F. Sols, A. S. Landsman, and M. Lewenstein, Wannier-Bloch approach to localization in high-harmonics generation in solids, Phys. Rev. X **7**, 021017 (2017).

[9] J. Li, J. Lu, A. Chew, S. Han, J. Li, Y. Wu, H. Wang, S. Ghimire, and Z. Chang, Attosecond science based on high harmonic generation from gases and solids, Nat. Commun. **11**, 2748 (2020).

[10] M. Mrudul, N. Tancogne-Dejean, A. Rubio, and G. Dixit, High-harmonic generation from spin-polarised defects in solids, npj Comput. Mater. **6**, 10 (2020).

[11] O. Schubert *et al.*, Sub-cycle control of terahertz high-harmonic generation by dynamical Bloch oscillations, Nat. Photon. **8**, 119 (2014).

[12] G. Vampa, T. Hammond, N. Thiré, B. Schmidt, F. Légaré, C. McDonald, T. Brabec, and P. Corkum, Linking high harmonics from gases and solids, Nature (London) **522**, 462 (2015).

[13] S. Cha *et al.*, Gate-tunable quantum pathways of high harmonic generation in graphene, Nat. Commun. **13**, 6630 (2022).

[14] H. K. Avetissian, G. F. Mkrtchian, and A. Knorr, Efficient high-harmonic generation in graphene with two-color laser field at orthogonal polarization, Phys. Rev. B **105**, 195405 (2022).

[15] M. S. Mrudul and G. Dixit, High-harmonic generation from monolayer and bilayer graphene, Phys. Rev. B **103**, 094308 (2021).

[16] R. Zhou, T. Guo, L. Huang, and K. Ullah, Engineering the harmonic generation in graphene, Mater. Today Phys. **23**, 100649 (2022).

[17] C. Liu, Y. Zheng, Z. Zeng, and R. Li, Polarization-resolved analysis of high-order harmonic generation in monolayer MoS_2, New J. Phys. **22**, 073046 (2020).

[18] B. Avchyan, A. Ghazaryan, K. Sargsyan, and K. V. Sedrakian, On laser-induced high-order wave mixing and harmonic generation in a graphene quantum dot, JETP Lett. **116**, 428 (2022).

[19] X. Zhang, T. Zhu, H. Du, H.-G. Luo, J. van den Brink, and R. Ray, Extended high-harmonic spectra through a cascade resonance in confined quantum systems, Phys. Rev. Res. **4**, 033026 (2022).

[20] A. D. Güçlü, P. Potasz, M. Korkusinski, P. Hawrylak, and P. Hawrylak, *Graphene Quantum Dots* (Springer, Heidelberg, 2014).

[21] S. Gnawali, R. Ghimire, K. R. Magar, S. J. Hossaini, and V. Apalkov, Ultrafast electron dynamics of graphene quantum dots: High harmonic generation, Phys. Rev. B **106**, 075149 (2022).

[22] B. Avchyan, A. Ghazaryan, K. Sargsyan, and K. V. Sedrakian, High harmonic generation in triangular graphene quantum dots, J. Exp. Theor. Phys. **134**, 125 (2022).

[23] S. Gnawali and V. Apalkov, High harmonic generation governed by edge states in triangular graphene quantum dots, Phys. Rev. B **108**, 115434 (2023).

[24] Y. Qin, X. Feng, and Y. Liu, Nonlinear refractive index in rectangular graphene quantum dots, Appl. Sci. **9**, 325 (2019).

[25] T. Brixner, G. Krampert, T. Pfeifer, R. Selle, G. Gerber, M. Wollenhaupt, O. Graefe, C. Horn, D. Liese, and T. Baumert, Quantum control by ultrafast polarization shaping, Phys. Rev. Lett. **92**, 208301 (2004).

[26] S. Kerbstadt, L. Englert, T. Bayer, and M. Wollenhaupt, Ultrashort polarization-tailored bichromatic fields, J. Mod. Opt. **64**, 1010 (2017).

[27] N. Tancogne-Dejean, O. D. Mücke, F. X. Kärtner, and A. Rubio, Ellipticity dependence of high-harmonic generation in solids originating from coupled intraband and interband dynamics, Nat. Commun. **8**, 745 (2017).

[28] R. Cireasa *et al.*, Probing molecular chirality on a sub-femtosecond timescale, Nat. Phys. **11**, 654 (2015).

[29] G. Sansone *et al.*, Isolated single-cycle attosecond pulses, Science **314**, 443 (2006).

[30] H. Mashiko, S. Gilbertson, C. Li, S. D. Khan, M. M. Shakya, E. Moon, and Z. Chang, Double optical gating of high-order harmonic generation with carrier-envelope phase stabilized lasers, Phys. Rev. Lett. **100**, 103906 (2008).

[31] X. Feng, S. Gilbertson, H. Mashiko, H. Wang, S. D. Khan, M. Chini, Y. Wu, K. Zhao, and Z. Chang, Generation of isolated attosecond pulses with 20 to 28 femtosecond lasers, Phys. Rev. Lett. **103**, 183901 (2009).

[32] S. Ghimire, A. D. DiChiara, E. Sistrunk, P. Agostini, L. F. DiMauro, and D. A. Reis, Observation of high-order harmonic generation in a bulk crystal, Nat. Phys. **7**, 138 (2011).

[33] B. Shan, S. Ghimire, and Z. Chang, Effect of orbital symmetry on high-order harmonic generation from molecules, Phys. Rev. A **69**, 021404(R) (2004).

[34] N. H. Burnett, C. Kan, and P. B. Corkum, Ellipticity and polarization effects in harmonic generation in ionizing neon, Phys. Rev. A **51**, R3418 (1995).

[35] C. Liu, Y. Zheng, Z. Zeng, and R. Li, Effect of elliptical polarization of driving field on high-order-harmonic generation in semiconductor ZnO, Phys. Rev. A **93**, 043806 (2016).

[36] Y. S. You, D. A. Reis, and S. Ghimire, Anisotropic high-harmonic generation in bulk crystals, Nat. Phys. **13**, 345 (2017).

[37] N. Yoshikawa, T. Tamaya, and K. Tanaka, High-harmonic generation in graphene enhanced by elliptically polarized light excitation, Science **356**, 736 (2017).

[38] S. A. Sato, H. Hirori, Y. Sanari, Y. Kanemitsu, and A. Rubio, High-order harmonic generation in graphene: Nonlinear coupling of intraband and interband transitions, Phys. Rev. B **103**, L041408 (2021).

[39] Z.-Y. Chen and R. Qin, Circularly polarized extreme ultraviolet high harmonic generation in graphene, Opt. Express **27**, 3761 (2019).

[40] T. Tamaya, A. Ishikawa, T. Ogawa, and K. Tanaka, Higher-order harmonic generation caused by elliptically polarized electric fields in solid-state materials, Phys. Rev. B **94**, 241107(R) (2016).

[41] M. Breusing, S. Kuehn, T. Winzer, E. Malic, F. Milde, N. Severin, J. P. Rabe, C. Ropers, A. Knorr, and T. Elsaesser, Ultrafast nonequilibrium carrier dynamics in a single graphene layer, Phys. Rev. B **83**, 153410 (2011).

[42] K. J. Tielrooij, J. C. W. Song, S. A. Jensen, A. Centeno, A. Pesquera, A. Zurutuza Elorza, M. Bonn, L. S. Levitov, and F. H. L. Koppens, Photoexcitation cascade and multiple hot-carrier generation in graphene, Nat. Phys. **9**, 248 (2013).

[43] D. Brida, A. Tomadin, C. Manzoni, Y. J. Kim, A. Lombardo, S. Milana, R. R. Nair, K. S. Novoselov, A. C. Ferrari, G. Cerullo, and M. Polini, Ultrafast collinear scattering and carrier multiplication in graphene, Nat. Commun. **4**, 1987 (2013).

[44] I. Gierz, J. C. Petersen, M. Mitrano, C. Cacho, I. C. E. Turcu, E. Springate, A. Stohr, A. Kohler, U. Starke, and A. Cavalleri, Snapshots of non-equilibrium Dirac carrier distributions in graphene, Nat. Mater. **12**, 1119 (2013).

[45] M. W. Graham, S.-F. Shi, D. C. Ralph, J. Park, and P. L. McEuen, Photocurrent measurements of supercollision cooling in graphene, Nat. Phys. **9**, 103 (2013).

[46] J. C. Johannsen, S. Ulstrup, F. Cilento, A. Crepaldi, M. Zacchigna, C. Cacho, I. C. E. Turcu, E. Springate, F. Fromm, C. Raidel, T. Seyller, F. Parmigiani, M. Grioni, and P. Hofmann, Direct view of hot carrier dynamics in graphene, Phys. Rev. Lett. **111**, 027403 (2013).

[47] J. C. Johannsen, S. Ulstrup, A. Crepaldi, F. Cilento, M. Zacchigna, J. A. Miwa, C. Cacho, R. T. Chapman, E. Springate, F. Fromm, C. Raidel, T. Seyller, P. D. C. King, F. Parmigiani, M. Grioni, and P. Hofmann, Tunable carrier multiplication and cooling in graphene, Nano Lett. **15**, 326 (2015).

[48] K. Ahnert and M. Mulansky, Odeint–Solving ordinary differential equations in C++, AIP Conf. Proc. **1389**, 1586 (2011).